Available online at www.sciencedirect.com

ScienceDirect

Energy Procedia 137 (2017) 487–496

Energy Procedia

www.elsevier.com/locate/procedia

14th Deep Sea Offshore Wind R&D Conference, EERA DeepWind'2017, 18-20 January 2017, Trondheim, Norway

Industrial scale turbine and associated wake development - comparison of RANS based Actuator Line Vs Sliding Mesh Interface Vs Multiple Reference Frame method.

Mandar Tabib[a,*], M Salman Siddiqui[b], Adil Rasheed[a], Trond Kvamsdal[b]

[a]*Mathematics and Cybernetics, SINTEF Digital, Strindveien 4, 7035, Trondheim, Norway.*
[b]*Department of Mathematical Sciences,Faculty of Information Technology and Electrical Engineering,NTNU,Trondheim,Norway.*

Abstract

This current work compares the three methodologies (Actuator Line model (ALM), Sliding Mesh Interface (SMI) and Multiple Reference Frame (MRF)) in modeling an industrial scale reference turbine at different tip speed ratios (TSR). The comparison shows that all the 3 models qualitatively predict the expected trend of power coefficient (C_p) vs TSR curve with an optima around $TSR \approx 7.5$. But the quantitative values of the predicted C_p, the wake deficits and the flow patterns differ from model to model. Between ALM and MRF, the former predicts a relatively milder variation of C_p with TSR. A deeper analysis of the flow pattern and wake deficit behind the turbine helps in understanding the behavioral characteristics of these models. MRF shows variations in flow pattern with TSRs, like the associated stall conditions at $TSR = 6$ and an optimum angle of attack condition at $TSR = 7.5$. ALM shows only a slight variation in the flow pattern near the hub region (DU40 location) at different TSRs. This is because the blades are not resolved in ALM. Perhaps, such differences in flow-pattern predictions result in the differences in C_p vs TSR trends predicted by the MRF and ALM models. SMI, on the other hand, captures the complex 3D flow structures. The wake deficit comparison shows that both ALM and MRF model captures qualitatively higher wake deficit at $TSR = 7.5$ in the core wake region $0.8 > z/R > 0.2$ as compared to $TSR = 9$ and $TSR = 6$. This behavior too is related to the observed flow pattern as captured by these models. Future studies may involve using LES in ALM to see if it improves the RANS predictions.

Peer-review under responsibility of SINTEF Energi AS.

Keywords: CFD; wind turbine; 5MW NREL; ALM; SMI; MRF.

1. Introduction and work objectives

1.1. Introduction

Wind-turbine blades comprising of multiple airfoils exhibit complex flow patterns [1,2] along the blade length and generate wakes that influence a wind-farm operation [3,4]. It is important to model the flow accurately for enabling

* Corresponding author. Tel.: +4792011677.
E-mail address: mandar.tabib@sintef.no;adil.rasheed@sintef.no

1876-6102
Peer-review under responsibility of SINTEF Energi AS.
10.1016/j.egypro.2017.10.377

efficient designs of both the turbine and the wind-farm layout. However, conducting highly accurate flow simulations for industrial-scale turbine is time-consuming and industry often craves for faster simulation methodologies. There are different methodologies: Actuator Line Model (ALM), Sliding Mesh Interface (SMI) and Multiple Reference Frame (MRF) to model wind turbines and understand the associated wake dynamics. Wake dynamics have been shown to influence power production capabilities of downstream turbines depending upon the inter-turbine distance in a wind farm layout [1–5]. Amongst the three methodologies, the ALM has been used popularly to understand the wake dynamics in wind farms as it is computationally tractable to do so for multi-turbine set-ups. However, it is well-known that ALM does not explicitly resolve turbine blades and hence might not be expected to be accurate enough. On the other hand, the SMI approach resolves the blade and is expected to be more accurate but it is computationally intractable to perform for a set-up with multiple turbines. On other hand, the MRF is a steady state approach, and it employs a frozen rotor hypothesis (i.e. static blade) and involves the use of Coriolis and centrifugal forces in momentum equation to account for rotation. It will be interesting to compare the performance of these three methodologies to gain perspective on the performance of ALM methods, which will continue to be used for wind farms at least in the near future. In this regard, the current work compares the SMI, MRF and ALM methods for one industrial scale wind turbine. The objectives of this work can be enlisted as:

1.2. Objective

1. Verification of ALM, SMI and MRF model for the popular industrial scale NREL 5 MW reference turbine.
2. Comparing predictions of power coefficient C_p, flow pattern and wake deficit with varying tip speed ratios (TSR) using three different models.

The industrial scale turbine chosen for this work is NREL 5MW reference turbine [6]. NREL 5 MW turbine [6] [7] is a standardized industrial-scale off-shore turbine model, which consists of three $63m$ long blades defined in terms of eight cross sectional profiles (DU21, DU25, DU30, DU35, DU40 and NACA64) and twist angles at different locations away from the hub (as described in [6]).

These multiple-sections with diverse angles of attack provide an ideal opportunity to test and benchmark models and methodologies that can later be applied to solve a bigger range of industrial challenges. Hence, it is popularly used by leading groups (several of U.S. DOEs Wind and Hydro-power Technologies Programs, EU's UpWind research program, and the International Energy Agency (IEA)'s Wind Annex XXIII Subtask Offshore Code Comparison Collaboration) to test methodologies. Next we discuss the methods and approach.

2. Approach and Methods

The study is limited to the near wake region. The approach involves conducting a comparison and verification of ALM, MRF and SMI approaches at different tip speed ratios (TSR 6, 7.5 and 9). A RANS turbulence model is used. The SMI is done only at TSR=7.5 (the optimum tip speed ratio) owing to the computational efforts required for a moving mesh method. The verification involves a comparison of the predicted power coefficients trends, trends of wake decay behind turbine and flow pattern variation with different tip speed ratios. Due to lack of experimental data of wake deficit velocity profiles for NREL 5 MW reference turbine, it is not possible to do validation of the models, so we resort to a verification exercise. The governing equations and application details of SMI, ALM and MRF are explained next.

2.1. SMI approach

The conservation equations are solved on a moving mesh (a sliding mesh) to account for the turbine blade motion and to capture unsteady interactions between rotating part and stationary blades. This approach involves dividing the computational domain into a rotating and a stationary zone using a sliding interface. The approach assumes that the rotating computational mesh moves (or slides) relative to the stationary frame. The terms of the governing equations are integrated on a control volume, and the effect of the moving control volume is accounted by including the mesh motion flux in the computation of face mass fluxes in the convective terms (in other words the convective terms in the

governing equation are modied). Thus, the face mass fluxes in the convective terms have to be computed relative to the mesh motion flux (ie. the volume swept by moving cell face during its movement with the cell face velocity). This mesh motion flux is computed based on the space (or volume) conservation law, which ensures that the moving face velocity is calculated from the face-centered positions, such that the surface vectors as well as calculation volumes inside rotating part remain constant. The mesh position in the rotating domain is updated after every time step (as it changes with impeller rotation) and so are the cell face positions at the sliding interface. At the sliding interface, a conservative interpolation is used for both mass and momentum using a set of fictitious control volumes. The governing equations are solved only in an inertial reference frame. Following equations are solved throughout the domain for SMI approach using RANS turbulence model with standard wall function:

$$\nabla \cdot \mathbf{u_a} = 0 \tag{1}$$

$$\frac{\partial \mathbf{u_a}}{\partial t} + \nabla \cdot (\mathbf{u_a} \otimes \mathbf{u_a}) = -\nabla p + \nabla \cdot (\nu + \nu_t)\nabla(\mathbf{u_a} + (\nabla \mathbf{u_a})^{\mathbf{T}}) \tag{2}$$

2.2. Actuator Line Model

The turbine is modeled using actuator line model (ALM) approach, which was first developed by Sørensen and Shen [8]. The actuator line model (Equations 5, 6 and 7) uses the velocity field input from the CFD model and outputs body force, which is used as the sink term in the momentum equation. The momentum equation can be represented as 4, where **f** refers to external forces arising from actuator line model.

$$\nabla \cdot (\rho \mathbf{u}) = 0 \tag{3}$$

$$\frac{D\mathbf{u}}{Dt} = -\nabla\left(\frac{p}{\rho}\right) + \frac{1}{\rho}\nabla \cdot \mathbf{R} + \mathbf{f} \tag{4}$$

where, components of **R** can be computed as $R_{ij} = \nu_T\left(\frac{\partial u_i}{\partial x_j} + \frac{\partial u_j}{\partial x_i}\right) - \frac{2}{3}k\delta_{ij}$, where subscripts i, j refers to components of the vector, k is turbulent kinetic energy and ν_T ($=\mu_t/\rho$) is turbulent diffusivity.

The ALM approach resolves each blade of the turbine as a rotating line (made of N actuator segments), over which the forces are computed. The forces at each segment comprise of lift force and drag forces (Equations 5, 6), which are computed from the local relative velocity (V_{rel}), local twist angle, blade chord (c), local actuator width (w) and local angle of attack (α) at a given actuator segment. The local angle of attack is computed from the tangential and normal component of relative velocity at the segment. The lift coefficient (C_l) and drag coefficient (C_d) at each segment (in Equations 5, 6 and 7) are a function of the local angle of attack, and this dependency is provided as an input (blade airfoil data) to the ALM model. The force at an actuator segment i (f_i) is a point force and it is translated onto the fluid domain as a volumetric body force (F_i) using Gaussian projection (Equation 7). The regularization parameter (ε) in Equation 7 represents the width of the Gaussian and determines the concentration of the force. Larger the parameter, more smoothed out the force is on the flow field. The negative sign in Equation 7 accounts for the fact that the force exerted by the turbine on the flow field is equal and opposite to the force experienced by it due to the flow. At the location (x, y, z) of the fluid domain, the overall body force is summation of force over all N actuator segments of the turbine, where (x_j, y_j, z_j) is the location of the j^{th} segment and r_j is the distance between segment j and the fluid domain location.

$$L = \frac{1}{2}C_l(\alpha)\rho V_{rel}^2 cw \tag{5}$$

$$D = \frac{1}{2}C_d(\alpha)\rho V_{rel}^2 cw \tag{6}$$

$$F_i^T(x, y, z) = -\sum_{j=1}^{N} f_i^T(x_j, y_j, z_j, t)\frac{1}{\varepsilon^3\pi^{3/2}} exp\left[-\frac{r_j^2}{\varepsilon}\right] \tag{7}$$

2.3. Multiple Reference Frame

The governing Navier-Stokes equations are considered incompressible throughout the domain since the Mach number is always inside the limit of 0.3 in all the simulations. The governing equations are solved in an inertial reference frame with absolute velocity for the stationary zone of MRF constituting of turbine tower and nacelle. The following mass and momentum equations are solved:

$$\nabla \cdot \mathbf{u_a} = 0 \tag{8}$$

$$\nabla \cdot (\mathbf{u_a} \otimes \mathbf{u_a}) = -\nabla p + \nabla \cdot (\nu + \nu_t)\nabla(\mathbf{u_a} + (\nabla \mathbf{u_a})^{\mathbf{T}}) \tag{9}$$

where $\mathbf{u_a}$ is the absolute velocity as seen from a stationary reference frame.

To account for the affects of rotation inside the rotating zone, source terms are added in terms of coriolis and centrifugal forces. The equations are written in terms of the relative flow velocity $\mathbf{u_r}$, which is a resultant vector arises from the velocity triangle of incoming and the induced velocity from the turbine blade.

$$\nabla \cdot \mathbf{u_r} = 0 \tag{10}$$

$$\nabla \cdot (\mathbf{u_r} \otimes \mathbf{u_r}) + \mathbf{2\Omega} \times \mathbf{u_R} + \mathbf{\Omega} \times (\mathbf{\Omega} \times \mathbf{r}) = -\nabla p + \nabla \cdot (\nu + \nu_t)\nabla(\mathbf{u_r} + (\nabla \mathbf{u_r})^{\mathbf{T}}) \tag{11}$$

$$\mathbf{u_a} = \mathbf{u_r} + \mathbf{\Omega} \times \mathbf{r} \tag{12}$$

where $\mathbf{\Omega}$ is the rotational speed of the reference frame with respect to a stationary observer (here it will also be equal to the rotational speed of the turbine), p is pressure, ν is the kinematic viscosity of the air and ν_t is the turbulent kinetic viscosity.

2.4. Turbulence model

Regarding the numerical model, all the three approaches involve use of $k-\omega$ SST turbulence model[9] based on Reynolds Averaged Navier-Stokes. The turbulent diffusivity ν_T in the momentum transport equation (Equation 2,4,9) are computed by using this turbulence model. When $k-\omega$ model is used, the turbulent eddy viscosity is formulated in terms of turbulent kinetic energy (k) and specific dissipation (ω). The turbulent kinetic energy is obtained by solving equation 14 and specific dissipation is obtained by solving equation 15.

$$\mu_t = \frac{a_1 k}{max(a_1\omega, S F_1)} \tag{13}$$

$$\frac{Dk}{Dt} = \nabla \cdot \left(\frac{\nu_T}{\sigma_k}\nabla k\right) + P_k - \beta k\omega \tag{14}$$

$$\frac{D\omega}{Dt} = \nabla \cdot \left(\frac{\nu_T}{\sigma_e}\nabla \omega\right) + P_k \frac{\gamma}{\nu_T} - \beta\omega^2 + 2(1-F_1)\nabla\omega\nabla k\frac{\sigma_{w2}}{\omega} \tag{15}$$

where σ_e and σ_e are turbulent prandtl numbers, P_k is production of turbulent kinetic energy due to shear.

$$P_k = \nu_T\left(\frac{\partial u_i}{\partial x_j} + \frac{\partial u_j}{\partial x_i}\right)\frac{\partial u_i}{\partial x_j} \tag{16}$$

2.4.1. Numerical implementation - Computational domain, mesh and parameters

Figure 1 shows the computational domain, mesh and suitability of mesh. The domain size for SMI and ALM simulations (figure 1(a) and 1(b)) are kept similar: $200m \times 120m(streamwise) \times 200m$ for SMI and $200m \times 190m(streamwise) \times 200m$ for ALM. While MRF uses a 120^0 sector with rotational periodicity and the dimensions of the domain are shown in figure 1(c) . Regarding mesh size, SMI uses a mesh of 8 million cell elements comprising of mostly tetrahedral cells with few layers of prismatic cells to capture the blade boundary layer region, while the ALM uses a grid of 1.5 Million cells with about 40 grid points across the rotor diameter (thus minimum grid length is about $3m$). This grid

should be sufficient to resolve wake tip vortex. MRF uses a mesh size of 2.8 Million. For SMI and MRF, the blade surface has been treated as a wall with no-slip boundary and employs a wall function based on Spalding's law [10] that gives a continuous kinematic viscosity profile to the wall over wide range of y^+. This is required because the average y^+ value near blade wall is 667 while the minimum y^+ value is 11 and in terms of grid size - the minimum wall normal grid size is $0.008m$ near the blade. Simulations are conducted with a uniform inlet wind velocity of $9m/s$ applied on the inlet face at different TSRs. The TSR is changed by adjusting the rotational speed of the turbine while keeping the inlet wind velocity constant. At the outlet face, a standard outlet boundary condition is used (fixed pressure value and zero normal gradient for rest). A free slip boundary condition is applied on the rest of the surfaces. For the actuator line method, about 40 actuator segments (i.e parameter N in equation 7) were used in the simulation. The regularization parameter (ϵ in equation 7) in ALM is chosen to be about two times the cube root of grid volume size in that region. This is selected so as to ensure that the force is not overly concentrated to cause numerical oscillations / solver instability, and neither does the force becomes too smoothed so as to cause no resistance to the wind flowing through the turbine. For ALM, the RANS results are run for $100s$ of simulation time (which corresponds to the passage of 17

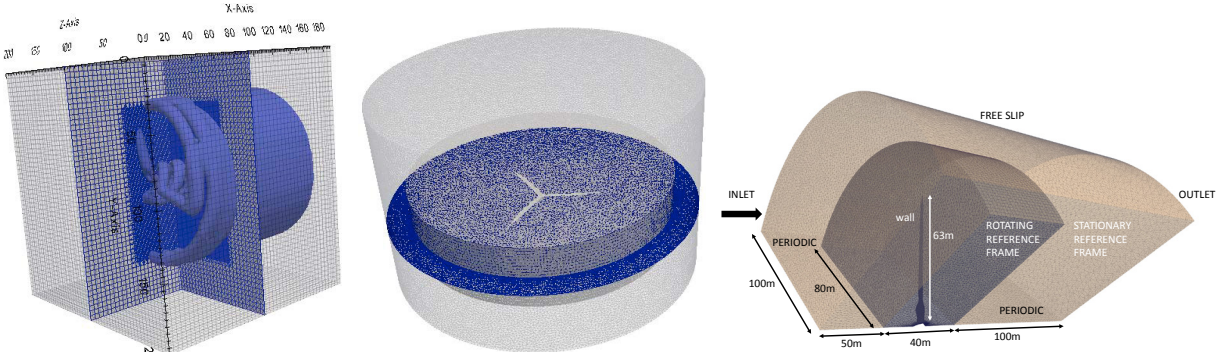

(a) ALM (b) SMI (c) MRF

Fig. 1. Domain and mesh for ALM,SMI and MRF

revolutions of the turbine and approximately 5 times flow passage through domain at wind free stream velocity). The ALM simulations run at a time step of around $0.007s$ (corresponding to courant number of 0.1 which is constrained by the tip speed). The averaging was done for last $100s$. The ALM simulations are run with 16 cores on a 3.2 GHz Intel(R) Xeon (R) CPU machine and took one week of computational time. For SMI, the RANS results are run for a total time of $23.45s$ corresponding to about four revolutions (and the flow developed after 3 revolutions). All the SMI RANS computations are performed on 256 cores of a 2.6GHz Intel(R) Xeon(R) CPU machine on *Vilje*, the high performance computational facility at Norwegian University of Science and Technology. The simulation time-step reached a lower value of 10^{-5} s in order to maintain the Courant number of 1. The simulation took around 3 weeks of computation time on the *Vilje*. The MRF was run till the time a steady state solution was obtained , wherein the convergence criteria was that the residual error for each variable (U,p,k,ϵ) falls below a prescribed value (around $5x10^{-4}$.

2.5. Solver details

Regarding solver, OpenFOAM was used in all the simulations. The OF uses an elliptic equation for the modified pressure which involves combining the continuity equation with divergence of momentum equation. This elliptic equation along with the momentum equation and turbulence equation are solved in a segregated manner using the Semi-Implicit Method for Pressure-Linked Equations (SIMPLE) algorithm. The OF uses a finite volume discretization technique, wherein all the equations are integrated over control volumes (CV) using Green Gauss divergence theorem. The gauss divergence theorem converts the volume integral of divergence of a variable into a surface integral of the variable over faces comprising the CV. Thus, the divergence term defining the convection terms can simply be computed using the face values of variables in the CV. The face values of variables are obtained from their neighboring cell centered values by using convective scheme. In this work, all the equations (except k_{sgs}) use second order linear

discretization scheme, while the turbulent equations use upwind convection schemes. Similarly, the diffusion term involving Laplacian operator (the divergence of the gradient) is simplified to compute the gradient of the variable at the face. The gradient term can be split into contribution from the orthogonal and the non-orthogonal parts, and both these contributions are accounted for.

3. Results and discussions

3.1. Verification study: Power coefficient (C_p) Vs tip speed ratio(TSR)

Jonkman et.al.([6]) studied the evolution of the power coefficient as a function of the TSR and the blade-pitch for case of NREL 5 MW reference turbine. This work was done using the FAST model involving the AeroDyn module. From these simulations, they found that the peak power coefficient of 0.482 occurred at a TSR of 7.55 and at a rotor-collective blade-pitch angle of 0.0°. A similar study has been carried out by Rannam Chaaban (data available at https://wind.nrel.gov/forum/wind/viewtopic.php?t=582) and he predicted the optimum C_p to occur at TSR=8. Rannam's study has been used for the verification of our ALM, MRF and SMI model (as shown in Figure 2). The ALM method also provides an optimum power coefficient at the TSR of 7.5 but it under-predicts the optimum power coefficient value (around 0.42). Also, the variation in C_p with varying TSR is small (almost flatter, though a peak in C_p can be seen at TSR 7.5)as compared to the FAST model. The MRF is also able to predict the optimum C_p at 7.5 but it over-predicts the C_p as compared to the FAST simulation. It is possible to obtain similar results as FAST by tuning regularization parameter ϵ. However, this is not done in the current work as it's a verification exercise and not a validation exercise, and all models can differ from the exact experimental observation (which are currently not available for NREL 5 MW reference turbine). The SMI method predicts a $C_p = 0.51$ at $TSR = 7.5$. The reasons for the observed C_p vs TSR variations for these different models is explained while comparing the flow patterns in section 3.3 and wake deficit in section 3.2. Further, the SMI predicts a higher 3D flow nature in the region behind turbine

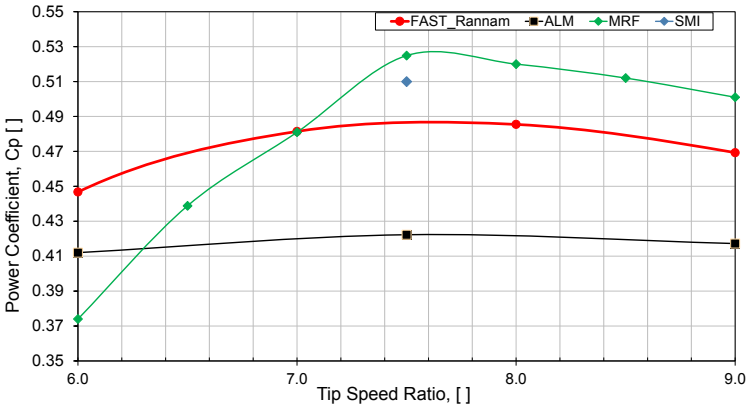

Fig. 2. Verification - power coefficient versus tip speed ratio for ALM, MRF, SMI and FAST models.

as compared to the AMI (as seen in streamlines in figure 6). This limitation can also be attributed to the distributed nature of force projection in ALM methodology along with the conditions of non-explicit resolution of the blade . However, despite these limitations, ALM has been able to predict the trends in wake deficit and power coefficients.

3.2. Comparison of wake dynamics with tip speed ratios

Wind deficit variation with tip speed ratio have been analyzed at six different locations behind the turbine (0.15R, 0.3R, 0.45R, 0.6R, 0.9R and 1.3R, where R refers to the radius of turbine = 63m). Figure 3-figure 4 together shows the mean wind deficit variations predicted at different TSR by different models. The *X-axis* represent wake deficit [$\Delta U/U_{inflow} = (U_{inflow}\text{-}U)/U_{inflow}$] in all the figures. The wake regions should have positive wake deficit if the hub and blades are modelled correctly. Figure 3 shows the wake deficit predicted by the three methods (ALM with a fine and

a coarse mesh for grid dependency, SMI and MRF) for a single tip speed ratio of 7.5 at two locations downstream of the turbine (0.3R and 0.9R). The trends at these two locations are similar to the six locations that have been analyzed (but not shown in the paper for sake of brevity). Figure 3 shows that the finer mesh ALM is closer to the results of MRF and SMI as the projection of forces and resolution of velocity gradients is better. In regions near tip vortex ($0.9R > z/R > 1.1$), the finer ALM shows a sharp velocity gradient corresponding to the presence of shear region accompanying tip vortex. Even the finer ALM model is seen to differ from MRF and SMI models in 2 major ways: (a) at the near the hub axis region ($0.25 > z/R > -0.25$) along the six downstream locations (figure 3 shows for 2 locations), the ALM model suggests a higher wind velocity and a negative wake deficit as the hub is not modelled in this case, whereas for MRF and SMI, a higher wake deficit in this near hub region is seen as the hub is explicitly modeled. (b) at the core wake region ($1 > z/R > 0.3$) along the six downstream locations (figure 3 shows for 2 locations), the ALM model predicts higher wake deficit than MRF and SMI. In other words, the MRF and SMI models show faster wake recovery than the ALM.

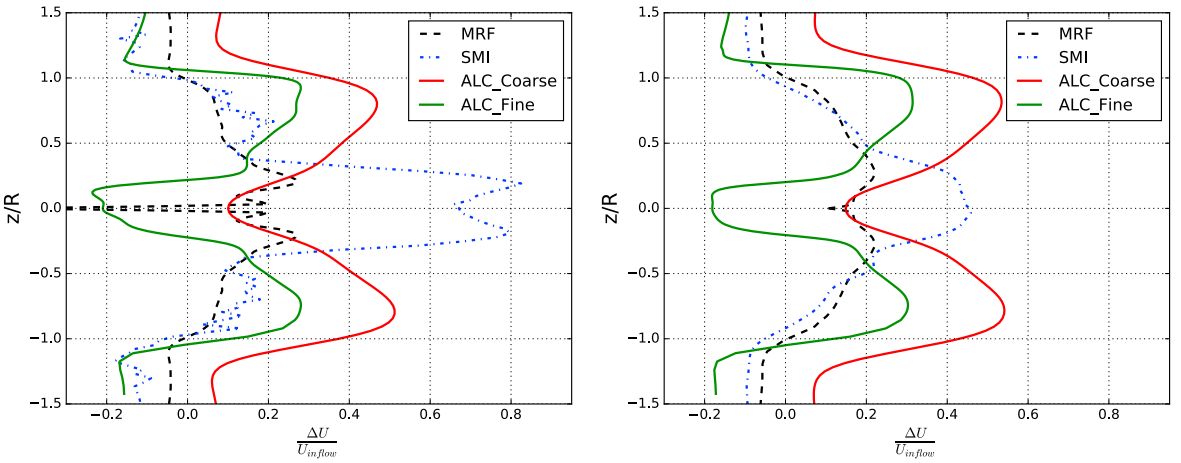

(a) TSR 7.5 at 0.3R downstream (b) TSR 7.5 at 0.9R downstream

Fig. 3. Wake deficit profiles predicted by ALM, MRF and SMI. Similar trends exist till 1.3R downstream distance.

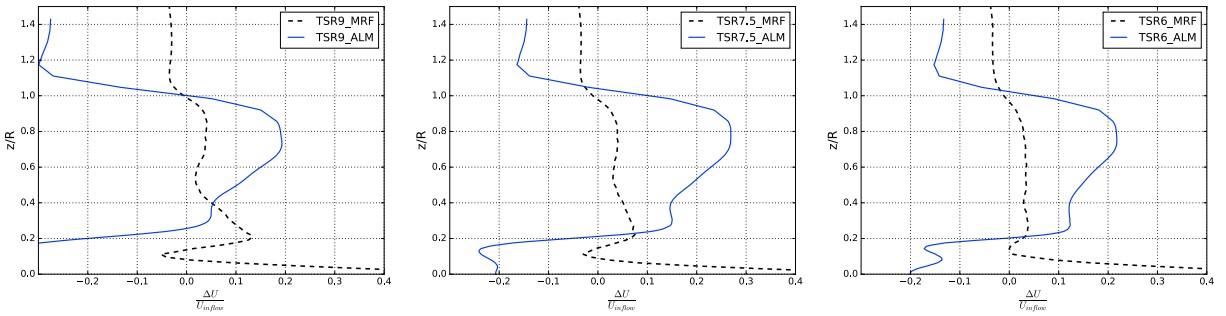

(a) TSR 9 at 0.15R - MRF Vs. ALM (b) TSR 7.5 at 0.15R - MRF Vs. ALM (c) TSR 6 at 0.15R - MRF Vs. ALM

Fig. 4. Wake deficit profiles computed by ALM VS MRF at 3 TSRs - 9, 7.5 and 6. *X-axis* represents wake deficit $\Delta U/U_{inflow} = (U_{inflow}\text{-}U)/U_{inflow}$.

Next, we compare the predictive capability of ALM and MRF at various tip speed ratios (figure 4). Figure 4(a)-4(c) compares the predictive performance of both ALM and MRF for these three different TSRs at 0.15R. The ALM and MRF are predicting a higher wake deficit at $TSR = 7.5$ in the core wake region $0.8 > z/R > 0.2$ as compared to

$TSR = 9$ and $TSR = 6$. At an optimum TSR of 7.5, more energy is extracted by the blades in that region leading to higher wind deficit and also higher C_p, while as we increase or decrease the tip speed ratio (towards 9 or 6), the energy extracted is lesser resulting in lower wind deficit and lower C_p. In all cases, the blade-tip region contributes more torque and hence power than the hub region. The energy extracted by a blade is associated with the flow pattern (as described in section 3.2. The ALM is over-predicting wake deficit in the core wake region as compared to the MRF. But, still the ALM predicts lower C_p values than MRF. It could be perhaps due to two reasons: (a) the higher wake deficit predicted by MRF in the $0.25 > z/R$ region as compared to the ALM case compensates for the lower wake deficit behavior in the core wake region $0.8 > z/R > 0.25$; (b) wake-recovery - the condition at turbine downstream (x=0.15R downstream) may not truly reflect the condition at the turbine blade location (located at x=0R, where C_p is measured). This could be due to the difference in wake-recovery/wake-growth from 0R to 0.15 R as predicted by ALM and MRF case. Next, we compare the flow patterns predicted by MRF and ALM approach and relate it to the observation on C_p and wake deficit.

3.3. Comparison of flow pattern by MRF and ALM

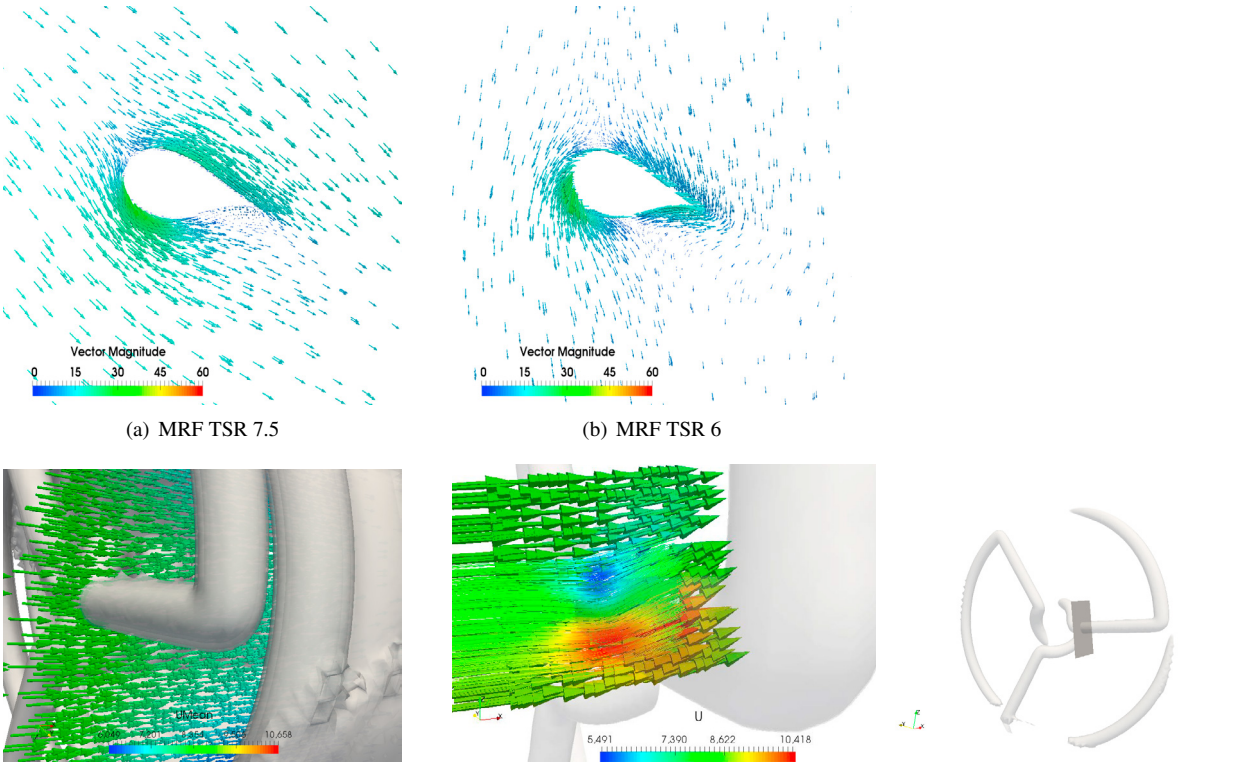

(a) MRF TSR 7.5 (b) MRF TSR 6

(c) ALM TSR 7.5 (d) ALM TSR 6 (e) Vorticity showing blades in ALM

Fig. 5. Prediction of impact of TSR on the flow pattern at the DU40 airfoil segment by MRF and ALM.

Figure 5 shows the change in flow pattern as the TSR varies as predicted by the MRF and the ALM methods. The comparison is shown for the DU40 airfoil segment that is located near the hub. The study of flow pattern across the blade helps to attribute the reason behind having an optimum TSR (in this case at TSR 7.5). Figure 5 shows that at TSR=6, the wind starts impinging on the top of the blade section instead of the leading edge, resulting in massive flow separation, while at TSR 7.5, the wind is inclined at an optimum angle of attack, and as the turbine reaches a TSR of 9 (not shown), the flow becomes more symmetric relative to the blade, and hence in both the cases (TSR 6 and TSR 9), the lift generated diminishes resulting in lower power coefficient (C_p) and the observed wake pattern. The MRF is able to capture this phenomenon (flow patterns in figure 5) as the blade is explicitly resolved. The ALM, on the

other hand, uses an input lift and drag coefficient value that varies with angle of attack to compute the resultant forces and this force is projected using gaussian distribution profile over a region. Hence, the deviation in flow patterns (varying angle of attack) with different TSRs is not as perceptible in the ALM predicted flow (figure 5(c)-5(d)) as in the MRF case. On comparing the ALM predicted pattern at TSR6 (figure 5(c)) with ALM predicted pattern at TSR 7.5 (figure 5(d)), a slightly higher angle of attack and a slightly higher deviation of flow across the DU40 region is seen in the TSR 6 case (figure 5(c)) as compared to the TSR 7.5 (figure 5(d)) case. This difference results in the milder variation in C_p as observed in figure 2. But the difference in variation of flow pattern and angle of attack is not as distinguishable as in the case of MRF. This is attributed to the inherent modelling aspects of the two cases as explain earlier. The location of DU40 airfoil segment in the blade is obtained in the case of ALM using vorticity contours as shown in figure 5(e). Further, the velocities do not reach as high in ALM case as in the MRF/SMI case (where

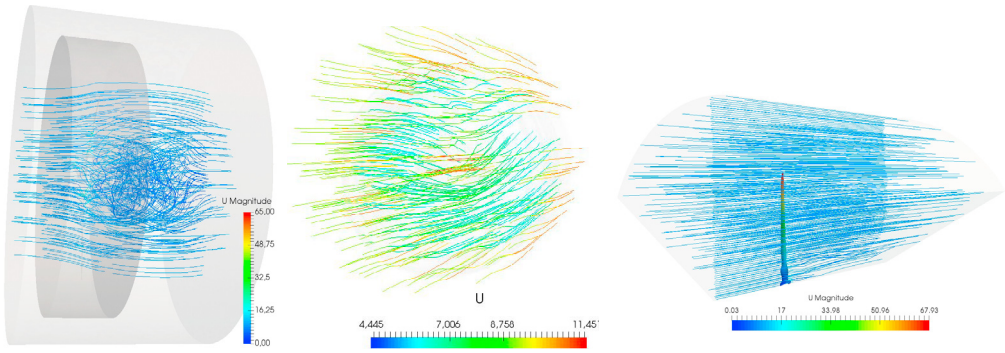

(a) SMI Streamline (b) ALM Streamline (c) MRF Streamline

Fig. 6. Streamlines predicted by SMI, ALM and MRF methods.

a high tip speed velocity is obtained). Further, the SMI (figure 6(a)) predicts a higher 3D flow nature in the region behind turbine as compared to the ALM (figure 6(b)) and MRF (figure 6(c)). This limitation can also be attributed to the distributed nature of force projection in ALM methodology along with the conditions of non-explicit resolution of the blade. MRF shows limited 3D rotatory effects as the blade is static and unsteadiness in flow is not captured. Due to these inherent modelling factors, the models have been predicting different quantitative wake deficit and power coefficients with tip speed ratios (as obtained in this work). These differences needs to be considered while using the model for wind farm/turbine designs.

4. Conclusion

The RANS turbulence based ALM and MRF models have been verified for their wake development and power coefficient predictions at 3 different tip speed ratios : (a) at an optimum TSR of 7.5, (b) at below the optimum TSR i.e. at $TSR = 6$ and (c) at higher than optimum TSR i.e. at $TSR = 9$). The computationally expensive SMI model is run only at the optimum TSR 7.5 and its results compared to ALM and MRF. Due to lack of experimental data for the industrial scale NREL 5 MW turbine, this work did not attempt to understand the accuracy of these models vis-a-vis experiments. Instead, the work focussed on noting the differences/similarities in predictions between these models based on their inherent modelling assumptions. Following conclusions can be drawn from the results :

- ALM-RANS and MRF-RANS method along with FAST model are qualitatively able to predict the expected trend in variation of C_p with TSR, and predict the optimum C_p at the TSR of 7.5-7.55 range. Though, quantitatively, these methods predict different optimum C_p values, which lies in the range of 0.42 - 0.52. SMI, conducted only at optimum TSR 7.5 case, predicts a C_p of 0.51. These quantitative variations between different models have been explained by the physics captured by them.
- Wake deficit comparison shows that both ALM and MRF model predict higher wake deficit at $TSR = 7.5$ in the core wake region $0.8 > z/R > 0.2$ as compared to the $TSR = 9$ and the $TSR = 6$. Though their quantitative

deficit values are different owing to inherent modelling factors. At an optimum TSR of 7.5, more energy is extracted by the blades in that region leading to a higher wake deficit and a higher C_p, while as we increase or decrease the tip speed ratio (towards 9 or 6), the energy extracted is lesser resulting in a lower wind deficit and a lower C_p. These variations with TSR are explained by observing the predicted flow pattern.

- Flow-pattern - The SMI shows more complex 3D nature of flow as compared to MRF and ALM at $TSR = 7.5$. The MRF-RANS shows variation in flow pattern with varying TSRs which involves (a) prediction of stalling condition and the flow separation at $TSR = 6$ and (b) prediction of flow with an optimum angle of attack at $TSR = 7.5$. While the ALM-RANS only shows a slight variation in flow pattern in near hub region (DU40 location) due to variation in tip speed ratio. The change in angle of attack and flow deviation with changing TSR is not overly perceptible in ALM owing to the fact that the blade is not resolved. Perhaps, this is the reason for ALM predicting a milder variation of C_p with TSR as compared to the steeper slopes of C_p Vs TSR predicted by the MRF. However despite these limitations, the ALM has been able to follow the qualitative trend in wake deficit and power coefficient variation with tip speed, owing to the line source and the distributed nature of the force projection.

The comparison reveals quantitative differences and qualitative similarities in trends between 3 popular turbine models in the near-wake region. A modeler should consider this aspect when using a chosen model for designing turbine/farms. Future work involves comparison using LES models and study of far-wake regions.

Acknowledgements

The authors acknowledge the financial support from the Norwegian Research Council and the industrial partners of NOWITECH: Norwegian Research Centre for Offshore Wind Technology (Grant No.:193823/S60) (http://www.nowitech.no) and FSI-WT (Grant No.:216465/E20)(http://www.fsi-wt.no).

References

[1] F. Porté-Agel, Y. Wu, H. Lu, R. Conzemius, Large-eddy simulation of atmospheric boundary layer flow through wind turbines and wind farms., Journal of Wind Engineering and Industrial Aerodynamics (2011) 99(4): 154–168.

[2] M. V. Tabib, A. Rasheed, F. Fuchs, Analyzing complex wake-terrain interactions and its implications on wind-farm performance, Journal of Physics: Conference Series (2016) 753 (3), 032063.

[3] M. Churchfield, S. Lee, P. Moriarty, L. Martnez, S. Leonardi, G. Vijayakumar, J. Brasseur, A numerical study of the effects of atmospheric and wake turbulence on wind turbine dynamics, 50th AIAA Aerospace Sciences Meeting Including the New Horizons Forum and Aerospace Exposition (2012) 124 (2) 393–399.

[4] M. V. Tabib, A. Rasheed, , T. Kvamsdal, Les and rans simulation of onshore bessaker wind farm: analyzing terrain and wake effects on wind farm performance, Journal of Physics: Conference Series (2015) 625: 012032.

[5] M. V. Tabib, A. Rasheed, , T. Kvamsdal, Investigation of the impact of wakes and stratification on the performance of an onshore wind farm., Energy Procedia, 80 (2015) 302311.

[6] J. Jonkman, S. Butterfield, W. Musial, G. Scott, Definition of a 5mw reference wind tturbine for offshore system development., National Renewable Energy Laboratory Tech. Rep. NREL/TP-500e38060.

[7] H. Kooijman, C. Lindenburg, D. Winkelaar, E. Hooft, Dowec 6 mw pre-design: Aero-elastic modeling of the dowec 6 mw pre-design in phatas,, DOWEC Dutch Offshore Wind Energy Converter 1997-2003 Public Reports , DOWEC 10046-009, ECN-CX–01-135, Petten, the Netherlands: Energy Research Center of the Netherlands.

[8] J. Sørensen, W. Shen, Numerical modelling of wind turbine wakes., Journal of Fluids Engineering (2002) 124 (2) 393–399.

[9] A. Hellsten, Some improvements in menter's k-ω-sst turbulence model, 29th AIAA Fluid Dynamics Conference AIAA (1998) 2554.

[10] D. Spalding, A single formula for the law of the wall., Transactions ofth ASIDE, Series E: Journal of Applied Mechanics (1961) 28,455–458.